Research Article | Vol. 30, No. 18 / 29 Aug 2022 / Optics Express 31785
Optics EXPRESS

Resonant two-photon terahertz quantum cascade laser

MUHAMMAD ANISUZZAMAN TALUKDER,[1,*] PAUL DEAN,[2] EDMUND H. LINFIELD,[2] AND A. GILES DAVIES[2]

[1] *Department of Electrical and Electronic Engineering, Bangladesh University of Engineering and Technology, Dhaka- 1205, Bangladesh*
[2] *School of Electronic and Electrical Engineering, University of Leeds, Woodhouse Lane, Leeds LS2 9JT, United Kingdom*
[*] *anis@eee.buet.ac.bd*

Abstract: Lasers that can emit two photons from a single electron relaxation between two states of the same parity have been discussed since the early days of the laser era. However, such lasers have seen only limited success, mainly due to a lack of suitable gain medium. We propose that terahertz (THz) frequency quantum cascade lasers (QCLs) are an ideal semiconductor structure to realize such two-photon emissions. In this work, we present a THz QCL heterostructure designed to emit two resonant photons from each electronic relaxation between two same-parity states in the active region. We present coupled Maxwell-Bloch equations that describe the dynamics of such a two-photon laser and find analytical solutions for the steady-state light intensity, the steady-state energy-resolved carrier densities, and the total threshold carrier density. Due to the two-photon emission from each excited state relaxation and an increased photon-driven carrier transport rate, our simulations predict a significant enhancement of light intensity in our designed resonant two-photon THz QCL when compared to an exemplar conventional THz QCL structure.

1. Introduction

Lasers based on two-photon emission, in which a single electron relaxation between quantum levels of the same parity occurs through the simultaneous emission of two photons, were first proposed in the 1960s [1,2]. Such lasers are unique as a non-classical light source [3,4] and have been subject to a large theoretical effort [5–10] owing to the enormous potential they of fer for applications in frequency metrology, quantum gyroscopes, quantum cryptography, quantum communication, and in the generation of entangled photon pairs, in addition to many conventional frequency-specific applications of lasers [11,12]. To date, however, the potential of two-photon lasers remains largely unexplored as their experimental realization is challenging. The first successful demonstration of a two-photon laser was in 1987 using rubidium atoms for emission in the microwave frequency range [13], with the second and the last demonstration in 1992 using barium atoms for emission in the optical frequency range [14].

Semiconductor lasers are advantageous not least for their compactness and convenience, and two-photon semiconductor laser designs based on both interband [15,16] and intersubband transitions [17] have been investigated theoretically. Although two-photon spontaneous interband emission has been reported recently [18], a semiconductor-based two-photon laser has yet to be realized. While semiconductor technology based on interband transitions is more mature than that exploiting intersubband transitions, the latter offers more design flexibility as well as dipole moments typically ~10 times greater than those of interband transitions [17]. Such intersubband transitions are central to the operation of the quantum cascade laser (QCL) [19], which comprises a heterostructured semiconductor superlattice in which the electron transition energies are governed by the thickness and composition of alternating semiconductor materials, enabling operation across both the mid-infrared (mid-IR) and terahertz (THz) frequency ranges.

#467673 https://doi.org/10.1364/OE.467673
Journal © 2022 Received 13 Jun 2022; revised 28 Jul 2022; accepted 3 Aug 2022; published 15 Aug 2022

Optics EXPRESS

THz QCLs in particular are important sources for their proven and potential applications in biomedical imaging, molecular spectroscopy, astronomy, and security screening. Since their first demonstration in 2002 [20], THz QCLs have matured significantly in achieving high power and continuous wave operation [21,22], as well as enabling modelocked pulsed emission and the generation of stable frequency combs [23–25]. Nevertheless, many THz sensing applications and scientific endeavours would benefit from broader spectral emission as well as higher output powers without significant scaling of device dimensions and electrical driving powers.

We demonstrate here that THz QCLs are an ideal platform to realize a semiconductor laser based on two-photon emission. We present a practical heterostructure design for a resonant two-photon THz QCL based on the GaAs/AlGaAs material system. In our proposed two-photon active region, two cascaded photon emissions occur through relaxation of each excited electron; at the same time electrons cascade through subsequent heterostructure periods in the same way as a conventional QCL. Using a Maxwell-Bloch formalism to describe the laser dynamics, we derive expressions for the steady-state light intensity, steady-state energy-resolved carrier densities, and total carrier density required to reach the lasing threshold. We calculate the steady-state and threshold quantities for the designed two-photon THz QCL (designated '2P-QCL' hereafter) and compare this with a conventional one-photon THz QCL ('1P-QCL') when key parameter values vary. We find that not only does the 2P-QCL reach the lasing threshold with a lower carrier density than a comparative 1P-QCL, but also generates significantly more light intensity per heterostructure period with the same carrier density. Therefore, such 2P-QCL structures are expected to be characterised by broadband emission since they will support multiple modes simultaneously due to their ability to generate high gain, of fering the potential for devices with widely tunable emission, and high-temperature operation due to the two-photon emissions inherently being less affected by temperature rise. In this respect, our simulations indicate the potential of 2P-QCLs for the development of THz frequency comb sources offering greater dynamic range and higher spectral power densities.

Additionally, such 2P-QCL structures are expected to generate entangled photon pairs when the two photon transitions are not resonant, the photon energies are separated by more than the linewidth of photon transitions, and the dephasing time of the excited states is greater than the time required for the cascaded two-photon transition [17,26]. Many more exciting applications are also envisaged owing to their ability to generate entangled photon pairs [11,12]. However, the present work focuses on generating two resonant photons, each separately following linear optics, as opposed to the two photons presented in Refs. [12,13,14] that depend on nonlinear optics. On the other hand, the two photon energies in this work must be within the linewidth of each other's transition energies. Although the heterostructure layers can be grown with high accuracy with modern-day fabrication technologies, the resonance of the photon transitions needed to be maintained at the same bias could be challenging. Therefore, careful design-tuning and precise layer thicknesses will be required for the practical realization of the 2P-QCL.

2. Two-photon THz QCL structure

The conduction band energy diagram of one period of our designed 2P-QCL is shown in Fig. 1, in which the electronic states have been obtained by solving coupled Schrödinger-Poisson equations. The designed structure consists of two resonant gain stages, designated stages 'a' and 'b', cascaded in each active region unit; the upper energy level of stage 'a' acts as the lower energy level of stage 'b'. Therefore, the middle level in the three-level system is shared by both photon emissions in the cascade. Gain stage 'a', between levels 1 and 2, has a transition frequency of ~2 THz and a dipole matrix element of ~7 nm. Level 2 has a calculated non-radiative lifetime (τ_2) of ~50 ps, whereas level 1 has a non-radiative lifetime (τ_1) of ~0.5 ps, considering optical phonon, electron-electron, alloy-disorder, impurity, and interface roughness scattering rates. Gain stage 'b' is between levels 2 and 3, and also has a transition frequency of ~2 THz and a dipole moment

Optics EXPRESS

of ~7 nm. Level 3 also has a non-radiative lifetime (τ_3) of ~50 ps. We note that, crucial to a two-photon laser, levels 3 and 1 do not have a strong dipole moment between them owing to their identical parities. We also note that the lifetimes will depend on the operating temperature. In this work, we have assumed a temperature of 60 K. We also assumed a 0.162-nm mean roughness height and a 6-nm correlation length to calculate the scattering rate due to the interface roughness [27].

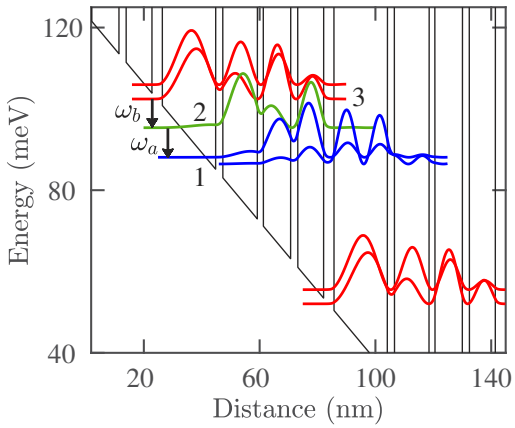

Fig. 1. Conduction band energy diagram and the moduli-squared wavefunctions of the designed 2P-QCL at an applied electric field of 8.5 kV/cm. The layer thicknesses of one period of alternating $Al_{0.15}Ga_{0.85}As$/GaAs materials are **1.8**, 9, **2.1**, 9.2, **4.6**, 18.5, **2.4**, and 12 nm, with the AlGaAs thickness given in bold font and GaAs thickness given in normal font.

Since $\tau_2 \approx \tau_3$, no population inversion will initially be established between levels 2 and 3. However, a strong population inversion will be established between levels 1 and 2 from the beginning since $\tau_2 \gg \tau_1$. Therefore, with sufficient current density, the stimulated radiative transitions will grow first in the gain stage 'a'. However, once this occurs, the radiative transition from level 2 to level 1 will reduce the level 2 lifetime to $\ll$50 ps, causing the population density of level 2 to reduce below that of level 3. A population inversion will therefore also be created between levels 2 and 3. When the photon density grows within the cavity, the carrier transport between levels 3 and 2 and between levels 2 and 1 will be dominated by radiative transitions and a strong population inversion will prevail in both gain stages. Therefore, during the relaxation of an excited electron from level 3 to level 1, two photons resonant in energy will be emitted. In Fig. 1, the uppermost red levels 3 and above it (3′) and bottom blue levels 1 and below it (1′) are degenerate states. Therefore, 3 and 3′ and 1 and 1′ will work as mixed states in the degenerate limit, and hence, as single levels. Therefore, in a 3-level approximation, levels 3 and 3′ and 1 and 1′ are treated as single levels.

3. Theoretical model

3.1. Maxwell-Bloch equations

To develop a mathematical model of the proposed resonant 2P-QCL, we use Maxwell-Bloch equations that take into account the coherent interactions between the field and the gain medium, which cannot be included in a rate equation formulation. Coherent interactions are important in QCLs and Maxwell-Bloch equations have been used to successfully reproduce the experimentally observed phenomena. In this approach, the dynamics of polarization and population inversion are described by the Bloch equations, while the propagation of field is described by the Maxwell

Optics EXPRESS

equation. We assume that levels 1 and 2 forming gain stage 'a' are coupled by a dipole moment d_a that decays in a characteristic dephasing time T_{2a}. Similarly, levels 2 and 3 in gain stage 'b' are coupled by a dipole moment d_b that decays in a characteristic dephasing time T_{2b}. The polarization densities η_a and η_b in gain stages 'a' and 'b' can be given by Bloch equations [26,28]

$$\frac{\partial \eta_{a\pm}}{\partial t} = \frac{id_a}{2\hbar}\left[(\rho_2-\rho_1)E_{\pm}+(\rho_2^{\mp}-\rho_1^{\mp})E_{\mp}\right]-\frac{\eta_{a\pm}}{T_{2a}}, \tag{1a}$$

$$\frac{\partial \eta_{b\pm}}{\partial t} = \frac{id_b}{2\hbar}\left[(\rho_3-\rho_2)E_{\pm}+(\rho_3^{\mp}-\rho_2^{\mp})E_{\mp}\right]-\frac{\eta_{b\pm}}{T_{2b}}, \tag{1b}$$

where E is the envelope of the electric field, ρ_x is the population density in level x, $\rho_x^{\pm}$ is the grating created on the population density in level x due to the interaction between the forward and backward traveling electric fields, and $\hbar$ is the Planck's constant. We use a subscript + (−) to denote a quantity that is related to the field propagating in the positive (negative) z-direction.

The change in carrier densities due to emission stimulated by a propagating electric field and non-radiative relaxation can be described by [26,28]

$$\frac{\partial \rho_1}{\partial t} = -\lambda-\frac{id_a}{2\hbar}(E_+^*\eta_{a+}+E_-^*\eta_{a-}-\text{c.c.})+\frac{\rho_2}{\tau_2}, \tag{2a}$$

$$\frac{\partial \rho_2}{\partial t} = -\frac{id_b}{2\hbar}(E_+^*\eta_{b+}+E_-^*\eta_{b-}-\text{c.c.})+\frac{id_a}{2\hbar}(E_+^*\eta_{a+}+E_-^*\eta_{a-}-\text{c.c.})-\frac{\rho_2}{\tau_2}+\frac{\rho_3}{\tau_3}, \tag{2b}$$

$$\frac{\partial \rho_3}{\partial t} = \lambda+\frac{id_b}{2\hbar}(E_+^*\eta_{b+}+E_-^*\eta_{b-}-\text{c.c.})-\frac{\rho_3}{\tau_3}, \tag{2c}$$

$$\frac{\partial \rho_1^{\pm}}{\partial t} = -\frac{id_a}{2\hbar}(E_{\pm}^*\eta_{a\mp}-E_{\mp}\eta_{a\pm}^*)-\frac{\rho_1^{\pm}}{\tau_1}, \tag{2d}$$

$$\frac{\partial \rho_2^{\pm}}{\partial t} = -\frac{id_b}{2\hbar}(E_{\pm}^*\eta_{b\mp}-E_{\mp}\eta_{b\pm}^*)+\frac{id_a}{2\hbar}(E_{\pm}^*\eta_{a\mp}-E_{\mp}\eta_{a\pm}^*)-\frac{\rho_2^{\pm}}{\tau_2}+\frac{\rho_3^{\pm}}{\tau_3}, \tag{2e}$$

$$\frac{\partial \rho_3^{\pm}}{\partial t} = \frac{id_b}{2\hbar}(E_{\pm}^*\eta_{b\mp}-E_{\mp}\eta_{b\pm}^*)-\frac{\rho_3^{\pm}}{\tau_3}, \tag{2f}$$

where λ is the injection or pumping rate to level 3 and the extraction rate from level 1 given by ρ_1/τ_1. Here, we assume that the extracted carriers from level 1 are injected only to level 3. Although the injection rate from level 1 to 3 will be ~100% in a well-designed THz QCL structure, there could be carriers injected to level 2 from 1. However, in both the 1p- and 2P-QCLs, the injection of carriers from level 1 to 2 will not change the results in either case. The lifetime τ_1 is very short due to the ultra-fast phonon depopulation. Since the inverse of transition rate between any two levels is $\gg \tau_1$ and the characteristic radiative decay time during lasing, we have assumed $\tau_2 = \tau_{21}$ and $\tau_3 = \tau_{32}$ in this work. We note that although these assumptions simplify the analytical approach, the results do not vary much if τ_{31} or the upward transitions are considered. In particular, we have simulated the Maxwell-Bloch equations without these assumptions using a finite-difference time-domain (FDTD) technique and found similar results.

The evolution of the electric field can be given by Maxwell's equation [26,28]

$$\frac{n}{c}\frac{\partial E_{\pm}}{\partial t} = \mp\frac{\partial E_{\pm}}{\partial z}-i\frac{N_a\Gamma d_a k}{\epsilon_0 n^2}\eta_{a\pm}-i\frac{N_b\Gamma d_b k}{\epsilon_0 n^2}\eta_{b\pm}-lE_{\pm}, \tag{3}$$

where n denotes the index of refraction, c denotes the speed of light, ϵ_0 denotes the vacuum permittivity, N_a and N_b denote the electron densities in gain stages 'a' and 'b,' respectively, Γ denotes the overlap factor between the laser mode and the active region, l denotes the linear cavity loss per unit length not including mirror losses, and k denotes the wave number associated with the THz radiation. The carrier densities N_a and N_b are related to the total carrier density in a period N by $N_a = N(\rho_2-\rho_1)$ and $N_b = N(\rho_3-\rho_2)$.

Optics EXPRESS

3.2. Steady-state solutions

We proceed by solving the coupled Eqs. (1)–(3) to find analytical steady-state solutions for polarization, population density, and electric field. We also derive an analytical expression for the threshold carrier density for lasing for the designed 2P-QCL structure. At steady-state, we can assume $E_+(t) = E_-(t) = \bar{E}$, $\eta_{a+}(t) = \eta_{a-}(t) = \bar{\eta}_a$, $\eta_{b+}(t) = \eta_{b-}(t) = \bar{\eta}_b$, $\rho_1(t) = \bar{\rho_1}$, $\rho_2(t) = \bar{\rho_2}$, $\rho_3(t) = \bar{\rho_3}$. Since we are interested only in the steady-state output intensity, rather not on the spectra, we can ignore the inversion gratings, and set $\rho_1^{\pm}(t) = 0$, $\rho_2^{\pm}(t) = 0$, and $\rho_3^{\pm}(t) = 0$. By setting the time derivatives to zero in Eq. (1), we can solve $\bar{\eta}_a$ and $\bar{\eta}_b$ as

$$\bar{\eta}_a = i\frac{d_a}{2\hbar}T_{2a}(\bar{\rho}_2 - \bar{\rho}_1)\bar{E}, \tag{4a}$$

$$\bar{\eta}_b = i\frac{d_b}{2\hbar}T_{2b}(\bar{\rho}_3 - \bar{\rho}_2)\bar{E}. \tag{4b}$$

Now, substituting $\bar{\eta}_a$ and $\bar{\eta}_b$ in Eq. (3), we obtain a steady-state relation between the gain generated in each gain stage and the total loss given by

$$g_a(\bar{\rho}_2 - \bar{\rho}_1) + g_b(\bar{\rho}_3 - \bar{\rho}_2) - l_t = 0, \tag{5}$$

where $g_a = N_a\Gamma d_a^2 k T_{2a}/(2\epsilon_0 n^2\hbar)$ and $g_b = N_b\Gamma d_b^2 k T_{2b}/(2\epsilon_0 n^2\hbar)$ are the gains per unit length in gain stages 'a' and 'b,' respectively, l_t is the total loss per unit length including the mirror losses so that $l_t = l + \ln[1/(r_1 r_2)]/(2L_c)$, where r_1 and r_2 are the reflection constants of the two facets, and L_c is the laser cavity length.

At steady-state, we can rewrite Eq. (2) by substituting the expressions for $\bar{\eta}_a$ and $\bar{\eta}_b$ as

$$-\left(f_b\bar{E}^2 + \frac{1}{\tau_3}\right)\bar{\rho}_3 + f_b\bar{E}^2\bar{\rho}_2 + \frac{1}{\tau_1}\bar{\rho}_1 = 0, \tag{6a}$$

$$\left(f_b\bar{E}^2 + \frac{1}{\tau_3}\right)\bar{\rho}_3 - \left(f_a\bar{E}^2 + f_b\bar{E}^2 + \frac{1}{\tau_2}\right)\bar{\rho}_2 + f_a\bar{E}^2\bar{\rho}_1 = 0, \tag{6b}$$

$$\left(f_a\bar{E}^2 + \frac{1}{\tau_2}\right)\bar{\rho}_2 - \left(f_a\bar{E}^2 + \frac{1}{\tau_1}\right)\bar{\rho}_1 = 0, \tag{6c}$$

where $f_a = d_a^2 T_{2a}/(2\hbar^2)$ and $f_b = d_b^2 T_{2b}/(2\hbar^2)$. Additionally, $\bar{\rho}_1$, $\bar{\rho}_2$, and $\bar{\rho}_3$ are conserved in a closed three-level system such that $\bar{\rho}_1 + \bar{\rho}_2 + \bar{\rho}_3 = 1$. We can therefore solve $\bar{\rho}_1$, $\bar{\rho}_2$, and $\bar{\rho}_3$ as

$$\bar{\rho}_1 = \frac{\tau_1\left(1 + f_a\tau_2\bar{E}^2\right)\left(1 + f_b\tau_3\bar{E}^2\right)}{Z}, \tag{7a}$$

$$\bar{\rho}_2 = \frac{\tau_2\left(1 + f_a\tau_1\bar{E}^2\right)\left(1 + f_b\tau_3\bar{E}^2\right)}{Z}, \tag{7b}$$

$$\bar{\rho}_3 = \frac{f_b\tau_2\tau_3\bar{E}^2\left(1 + f_a\tau_1\bar{E}^2\right) + \tau_3\left(1 + f_a\tau_2\bar{E}^2\right)}{Z}, \tag{7c}$$

where Z is given by

$$\begin{aligned} Z =& \tau_2\tau_3 f_b\bar{E}^2\left(1 + f_a\tau_1\bar{E}^2\right) + \tau_3\left(1 + f_a\tau_2\bar{E}^2\right) \\ &+ \tau_2\left(1 + f_a\tau_1\bar{E}^2\right)\left(1 + f_b\tau_3\bar{E}^2\right) + \tau_1\left(1 + f_b\tau_3\bar{E}^2\right)\left(1 + f_a\tau_2\bar{E}^2\right). \end{aligned} \tag{8}$$

Now, substituting $\bar{\rho}_1$, $\bar{\rho}_2$, and $\bar{\rho}_3$ in Eq. (5), we find an equation for the steady-state light intensity ($\bar{E}^2$) in a resonant 2P-QCL given by

$$\begin{aligned} &3\tau_1\tau_2\tau_3 l f_a f_b\bar{E}^4 + \left[\left(\tau_1 + 2\tau_2\right)\tau_3 l_t f_b + \left(2\tau_1 + \tau_3\right)\tau_2 l_t f_a - \left(\tau_3 - \tau_1\right)\tau_2 g_b f_a\right. \\ &\left. - \left(\tau_2 - \tau_1\right)\tau_3 g_a f_b\right]\bar{E}^2 - \left[(\tau_2 - \tau_1)g_a + (\tau_3 - \tau_2)g_b - (\tau_1 + \tau_2 + \tau_3)l_t\right] = 0. \end{aligned}$$

Optics EXPRESS

Equation (9) reduces to an equation for $\bar{E}^2$ in a 1P-QCL when $d_b = 0$ as

$$(2\tau_1 + \tau_3)\tau_2 l_t f_a \bar{E}^2 - (\tau_2 - \tau_1)g_a + (\tau_1 + \tau_2 + \tau_3)l_t = 0. \tag{10}$$

3.3. Threshold condition

When the laser is driven at threshold, we can set $\bar{E} = 0$ and solve for the threshold carrier density N^{th}. Setting $\bar{E} = 0$ in Eq. (9) gives us

$$(\tau_2 - \tau_1)g_a^{\text{th}} + (\tau_3 - \tau_2)g_b^{\text{th}} - (\tau_1 + \tau_2 + \tau_3)l_t = 0, \tag{11}$$

where g_a^{th} and g_b^{th} are the gain coef ficients at threshold. Now, we can solve Eq. (11) for N^{th} as

$$N^{\text{th}} = \frac{2\epsilon_0 n^2 \hbar}{\Gamma k} \frac{(\tau_1 + \tau_2 + \tau_3)l_t}{(\tau_2 - \tau_1)(\rho_2 - \rho_1)d_a^2 T_{2a} + (\tau_3 - \tau_2)(\rho_3 - \rho_2)d_b^2 T_{2b}}. \tag{12}$$

When $\bar{E} = 0$, Eq. (6) reduces to simple rate equations where $\bar{\rho}_1$, $\bar{\rho}_2$, and $\bar{\rho}_3$ are related only by their non-radiative relaxation rates. By substituting $\bar{\rho}_1$, $\bar{\rho}_2$, and $\bar{\rho}_3$ by their expressions at $\bar{E} = 0$, we find an expression for N^{th} of a resonant 2P-QCL as

$$N^{\text{th}} = \frac{2\epsilon_0 n^2 \hbar}{\Gamma k} \frac{(\tau_1 + \tau_2 + \tau_3)^2 l_t}{(\tau_2 - \tau_1)^2 d_a^2 T_{2a} + (\tau_3 - \tau_2)^2 d_b^2 T_{2b}}. \tag{13}$$

For a 1P-QCL, N^{th} in Eq. (13) reduces to

$$N^{\text{th}} = \frac{2\epsilon_0 n^2 \hbar}{\Gamma k} \frac{(\tau_1 + \tau_2 + \tau_3)^2 l_t}{(\tau_2 - \tau_1)^2 d_a^2 T_{2a}}. \tag{14}$$

4. Results

We use the derived expressions to calculate N^{th}, $\bar{E}^2$, $\bar{\rho}_1$, $\bar{\rho}_2$, and $\bar{\rho}_3$ for the proposed 2P-QCL as well as a conventional, comparative 1P-QCL. To simulate the latter, we note that a 1P-QCL (with a single lasing transition corresponding to stage 'a' of our two-photon structure) is similar to the designed 2P-QCL except for the additional constraints that $d_b = 0$ and typically τ_3<50 ps. In this way, we can also vary N and τ_3 to investigate how the operating parameters of our designed 2P-QCL differ from those of a comparative 1P-QCL. We note that both 2P- and 1P-QCLs can be designed with varying number of quantum wells, and therefore, the period lengths may vary depending on the design principle. In Fig. 2, we show N^{th} in 2P- and 1P-QCLs as a function of τ_3 for three different values of τ_2. For these simulations, we assume a transition frequency of 2 THz with $d_a/e = d_b/e = 7$ nm, where e is the charge of an electron, $\tau_1 = 0.5$ ps, $T_{2a} = T_{2b} = 1$ ps, $L_c = 2$ mm, $l = 10$ cm^{-1}, $n = 3.3$, and $\Gamma = 1$. We note that N^{th} in the designed 2P-QCL is smaller than that in the 1P-QCL except when $\tau_2 \approx \tau_3$. In fact, while N^{th} increases with an increase of τ_3 for the 1P-QCL, in the case of the 2P-QCL, N^{th} significantly decreases when τ_3>τ_2. This observation can be understood by noting that although ρ_2 decreases as τ_3 increases, the population inversion between levels 1 and 2 is maintained and a population inversion is also established between levels 2 and 3 in the 2P-QCL with τ_3>τ_2. Therefore, under these conditions, photon emissions occurs in both gains stages 'a' and 'b', resulting in a decrease in N^{th}. In Figs. 3(a) and (b), we show $\bar{E}^2$ for the proposed 2P-QCL and 1P-QCL, respectively, as a function of N for different values of τ_3. The range of parameter values chosen here are typical in THz QCL designs. In both cases, we note that $\bar{E}^2$ increases when N increases, as expected. Crucially, however, we find that $\bar{E}^2$ is significantly greater in the proposed 2P-QCL than in the 1P-QCL. Although the relative increase of $\bar{E}^2$ in a 2P-QCL depends on the value of τ_3, $\bar{E}^2$ is enhanced at least by one order of magnitude for the τ_3 values considered in this work. This observation is

Optics EXPRESS

attributed directly to the two-photon nature of this structure, as explained in more detail below. We also find that $\bar{E}^2$ is largely invariant to changes in τ_3 in the proposed 2P-QCL, with $\bar{E}^2$ being slightly greater for greater τ_3 values. In 2P-QCL, the decrease in photon emission from gain stage 'a' when τ_3 increases is compensated by the additional photon emission from gain stage 'b.' In the 1P-QCL, however, although $\bar{E}^2$ is considerably smaller, its value increases by more than a factor of 6 when τ_3 changes from 50 ps to 10 ps, since a smaller τ_3 increases photon emission between levels 2 and 1, through an increase in $\bar{\rho}_2$. We note that this relative independence of $\bar{E}^2$ with respect to τ_3 in the 2P-QCL offers an important design flexibility. However, in practice, $\bar{E}^2$ cannot increase arbitrarily, rather will be limited by the increase of free-carrier absorption and temperature as N increases for both 1P- and 2P-QCLs. Additionally, the cascaded periods of QCLs will be misaligned at a higher N so that the carrier transport will suffer.

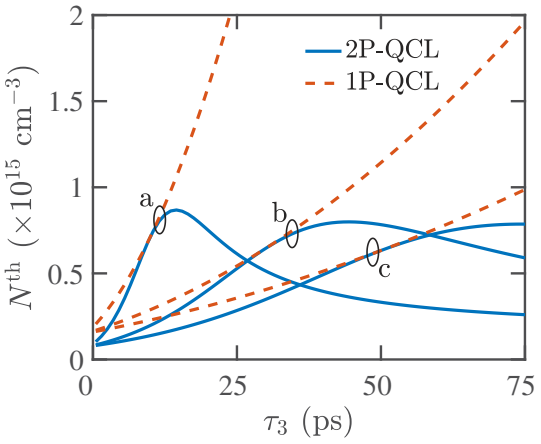

Fig. 2. N^{th} in 2P- and 1P-QCLs against τ_3 with τ_2 values (a) 10 ps, (b) 30 ps, and (c) 50 ps.

In Figs. 3(c) and (d), we show the changes in $\bar{\rho}_2$ and $\bar{\rho}_3$ in both the proposed 2P-QCL and the 1P-QCL as N and τ_3 vary. The change in $\bar{\rho}_1$ can be deduced as $\bar{\rho}_1 = 1 - \bar{\rho}_2 - \bar{\rho}_3$. Although $\bar{\rho}_2 \gtrsim \bar{\rho}_3$ in both structures before threshold, $\bar{\rho}_2 \ll \bar{\rho}_3$ after each laser reaches threshold due to stimulated emission from level 2 to level 1. In the 2P-QCL, the depletion of $\bar{\rho}_2$ and increased pumping to level 3 create population inversion between levels 2 and 3. Therefore, in Fig. 3(c), although $\bar{\rho}_3$ initially increases after threshold, it decreases with further increase of N as the photon density increases to saturate the gain. We also note that $\bar{\rho}_2$ decreases sharply after threshold and is driven into saturation due to a high photon density. By contrast, in the 1P-QCL, $\bar{\rho}_2$ decreases gradually with N as the photon density increases, although it is never driven into saturation. Also, $\bar{\rho}_3$ increases gradually with N due to increased pumping to level 3 and a fixed relaxation rate of level 3 irrespective of the photon density.

In the proposed 2P-QCL, two photon transitions deplete the carrier densities on fast timescales and carrier transport through the heterostructure is determined by photon-assisted transport. Therefore, the electrical pumping rate λ of the 2P-QCL is expected to be much greater than that of a 1P-QCL for a fixed N. This is illustrated in Fig. 4, which shows considerably greater λ in the 2P-QCL due to the high photon density in the cavity. The generation of two photons for each electron relaxation, together with this increased pumping rate, results in considerably greater output intensity for the 2P-QCL, as confirmed in Fig. 3(a).

To investigate the time-resolved dynamics of the 2P-QCL, we have solved the coupled Maxwell-Bloch Eqs. (1)–(3) using a numerical FDTD technique and found good agreements with the analytical results presented in this work. The dynamic output intensities ($|E_{\text{out}}|^2$) of 2P- and 1P-QCLs are shown in Figs. 5(a) and (b). The 2P-QCL shows stable dynamic output with a much

Optics EXPRESS

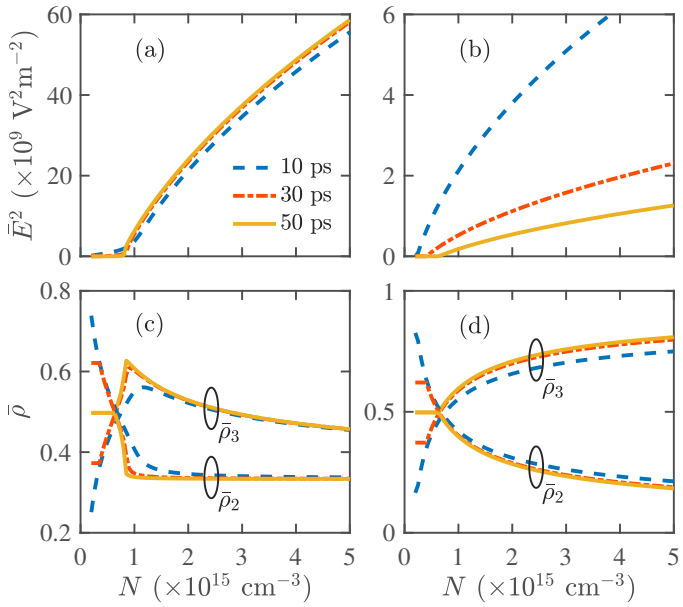

Fig. 3. $\bar{E}^2$ vs. N in (a) 2P- and (b) 1P-QCLs. Steady-state carrier densities $\bar{\rho}_2$ and $\bar{\rho}_3$ vs. N in (c) 2P- and (d) 1P-QCLs. The legends in (a) show values for τ_3 and apply for (a)–(d).

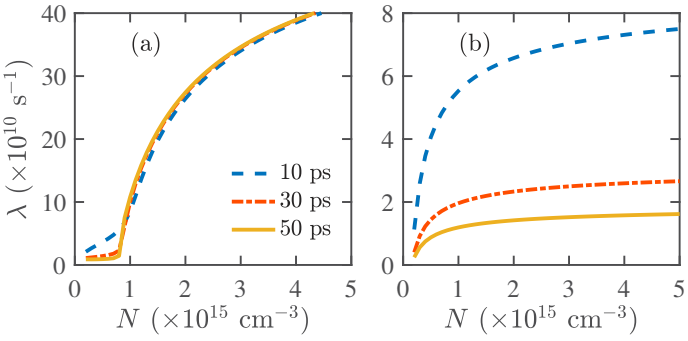

Fig. 4. λ for (a) 2P- and (b) 1P-QCLs when $\tau_2 = 50$ ps. The legends in (a) show values for τ_3 for both (a) and (b).

Optics EXPRESS

greater peak and average $|E_{\text{out}}|^2$ than 1P-QCL. We note that FDTD simulations show multimode instability in the 2P-QCL when $N \gg N^{\text{th}}$. In fact, we found >1.5 times broader output emission spectra in the 2P-QCL compared to that in the 1P-QCL for $\tau_2 = \tau_3 = 50$ ps and $N = 2 \times 10^{15}$ cm^{-3}, as shown in Figs. 5(c) and (d).

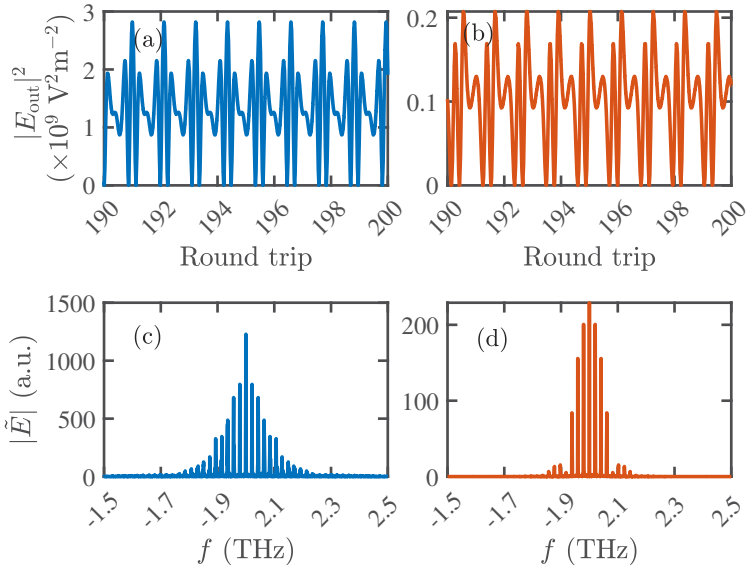

Fig. 5. Time-resolved output intensity ($|E_{\text{out}}|^2$) for (a) 2P- and (b) 1P-QCLs for several round trips. Emission spectra ($|\tilde{E}|$) for (c) 2P- and (d) 1P-QCLs. In each case, $N = 2 \times 10^{15}$ cm^{-3}.

5. Conclusion

In conclusion, we have presented a practical THz QCL design based on the GaAs/AlGaAs material system, which emits two-photons for each excited electronic state relaxation in the active region. We have solved the Maxwell-Bloch equations to derive the steady-state and threshold lasing conditions as key parameter values vary over a range that typically occurs in THz QCL structures. Our results show that the carrier densities become saturated and that carrier transport is dominated by photon-driven scattering due to the two-photon transitions in our structure. As such, the pumping rate is significantly greater than that in a comparative single-photon QCL, resulting in a significantly enhanced light intensity in our two-photon structure. Our design concept could open-up new opportunities for the development of high-power and broadband THz QCLs, as well as applications based on the generation of entangled photon pairs. This design could also help to reduce the adverse effects of temperature on THz QCLs. Since there are two cascaded photon transitions in the proposed structure, although the photon transition between the intermediate and lower levels will be affected by the temperature rise as it happens for conventional 1P-QCLs, the photon transition between the upper and intermediate levels will be less affected by the temperature rise. Therefore, the proposed 2P-QCL should lase at a much higher temperature than that reached by a 1P-QCL. We note that both 1P- and 2P-QCLs can be designed using different number of wells and their optimised performances may vary as well. Therefore, the relative superior performance of the 2P-QCL compared to 1P-QCL obtained in the systematic analysis presented in this work may also vary.

Funding. H2020 Future and Emerging Technologies (665158); H2020 Marie Skłodowska-Curie Actions (703912).

Optics EXPRESS

Disclosures. The authors declare no conflicts of interest.

Data availability. Data underlying the results presented in this paper are not publicly available at this time but may be obtained from the authors upon reasonable request.

References

1. P. P. Sorokin and N. Braslau, "Some theoretical aspects of a proposed double quantum stimulated emission device," IBM J. Res. Dev. **8**(2), 177–181 (1964).
2. A. M. Prokhorov, "Quantum electronics," Science **149**(3686), 828–830 (1965).
3. A. W. Boone and S. Swain, "Effective hamiltonians and the two-photon laser," Quantum Opt. **1**(1), 27–47 (1989).
4. A. W. Boone and S. Swain, "Theory of the degenerate two-photon laser," Phys. Rev. A **41**(1), 343–351 (1990).
5. F. V. Bunkin, "Two quantum transitions in optics," Soviet Physics JETP **23**, 1121–1123 (1966).
6. H. Schlemmer, D. Frölich, and H. Welling, "Two-photon amplification on cascade-transitions," Opt. Commun. **32**(1), 141–144 (1980).
7. M. Lewenstein, Y. Zhu, and T. W. Mossberg, "Two-photon gain and lasing in strongly driven two-level atoms," Phys. Rev. Lett. **64**(26), 3131–3134 (1990).
8. J. Zakrzewski, M. Lewenstein, and T. W. Mossberg, "Theory of dressed-state lasers. i. effective Hamiltonians and stability properties," Phys. Rev. A **44**(11), 7717–7731 (1991).
9. J. Zakrzewski, M. Lewenstein, and T. W. Mossberg, "Theory of dressed-state lasers. ii. phase diffusion and squeezing," Phys. Rev. A **44**(11), 7732–7745 (1991).
10. J. Zakrzewski, M. Lewenstein, and T. W. Mossberg, "Theory of dressed-state lasers. iii. pump-depletion effects," Phys. Rev. A **44**(11), 7746–7758 (1991).
11. H. Yuen and J. Shapiro, "Optical communication with two-photon coherent states–part i: Quantum-state propagation and quantum-noise," IEEE Trans. Inf. Theory **24**(6), 657–668 (1978).
12. O. Pfister, W. J. Brown, M. D. Stenner, and D. J. Gauthier, "Polarization instabilities in a two-photon laser," Phys. Rev. Lett. **86**(20), 4512–4515 (2001).
13. M. Brune, J. M. Raimond, P. Goy, L. Davidovich, and S. Haroche, "Realization of a two-photon laser oscillator," Phys. Rev. Lett. **59**(17), 1899–1902 (1987).
14. D. J. Gauthier, Q. Wu, S. E. Morin, and T. W. Mossberg, "Realization of a continuous-wave, two-photon optical laser," Phys. Rev. Lett. **68**(4), 464–467 (1992).
15. C. N. Ironside, "Two-photon gain semiconductor amplifier," IEEE J. Quantum Electron. **28**(4), 842–847 (1992).
16. D. H. Marti, M.-A. Dupertuis, and B. Deveaud, "Feasibility study for degenerate two-photon gain in a semiconductor microcavity," IEEE J. Quant. Electron. **39**(9), 1066–1073 (2003).
17. C. Z. Ning, "Two-photon lasers based on intersubband transitions in semiconductor quantum wells," Phys. Rev. Lett. **93**(18), 187403 (2004).
18. A. Hayat, P. Ginzburg, and M. Orenstein, "Observation of two-photon emission from semiconductors," Nat. Photonics **2**(4), 238–241 (2008).
19. J. Faist, F. Capasso, D. L. Sivco, C. Sirtori, A. L. Hutchinson, and A. Y. Cho, "Quantum cascade laser," Science **264**(5158), 553–556 (1994).
20. R. Köhler, A. Tredicucci, F. Beltram, H. E. Beere, E. H. Linfield, A. G. Davies, D. A. Ritchie, R. C. Iotti, and F. Rossi, "Terahertz semiconductor-heterostructure laser," Nature **417**(6885), 156–159 (2002).
21. S. Kumar, "Recent progress in terahertz quantum cascade lasers," IEEE J. Sel. Top. Quantum Electron. **17**(1), 38–47 (2011).
22. L. H. Li, L. Chen, J. R. Freeman, M. Salih, P. Dean, A. G. Davies, and E. H. Linfield, "Multi-watt high-power THz frequency quantum cascade lasers," Electron. Lett. **53**(12), 799–800 (2017).
23. D. Burghoff, T.-Y. Kao, N. Han, C. W. I. Chan, X. Cai, Y. Yang, D. J. Hayton, J.-R. Gao, J. L. Reno, and Q. Hu, "Terahertz laser frequency combs," Nat. Photonics **8**(6), 462–467 (2014).
24. S. Barbieri, M. Ravaro, P. Gellie, G. Santarelli, C. Manquest, C. Sirtori, S. P. Khanna, E. H. Linfield, and A. G. Davies, "Coherent sampling of active mode-locked terahertz quantum cascade lasers and frequency synthesis," Nat. Photonics **5**(5), 306–313 (2011).
25. F. Wang, H. Nong, T. Fobbe, V. Pistore, S. Houver, S. Markmann, N. Jukam, M. Amanti, C. Sirtori, S. Moumdji, R. Colombelli, L. Li, E. Linfield, G. Davies, J. Mangeney, J. Tignon, and S. Dhillon, "Short terahertz pulse generation from a dispersion compensated modelocked semiconductor laser," Lasers Photonics Rev. **11**(4), 1700013 (2017).
26. G. J. de Valcárcel, E. Roldán, J. F. Urchueguía, and R. Vilaseca, "Two-photon laser dynamics," Phys. Rev. A **52**(5), 4059–4069 (1995).
27. S. Tsujinoa, A. Borak, E. Müller, M. Scheinert, C. V. Falub, H. Sigg, and D. Grützmacher, "Interface-roughness-induced broadening of intersubband electroluminescence in p-sige and n-gainas/alinas quantum-cascade structures," Appl. Phys. Lett. **86**(6), 062113 (2005).
28. M. A. Talukder and C. R. Menyuk, "Quantum coherent saturable absorption for mid-infrared ultra-short pulses," Opt. Express **22**(13), 15608–15617 (2014).